Theoretical analysis the effect of material parameters on detectivity of $In_{0.53}Ga_{0.47}As$ photovoltaic detector

LI XU, YINGTIAN XU*, YONGGANG ZOU, HE ZHANG, YANG LI, XIN ZHAO, LIANG JIN, XIAOHUI MA, JINGZHI YIN[a]

State Key Laboratory of High Power Semiconductor Laser, Changchun University of Science and Technology, Changchun 130022, People's Republic of China

[a]*State Key Laboratory on Integrated Optoelectronics, College of Electronic Science and Engineering, Jilin University, 2699 Qianjin Street, Changchun, 130012, People's Republic of China*

In this paper, the dependence of detectivity on the direction of incident light, carrier concentrations, surface recombination velocities and material thicknesses for $In_{0.53}Ga_{0.47}As$ photovoltaic detector has been analyzed. When light injected from *p*-side, the *p*-region surface recombination velocity, its carrier concentration and thickness have significant impact to the detectivity. The *n*-region material parameters have slight impact on detectivity. The surface recombination velocity and its thickness influence is primarily for low carrier concentration ($n<10^{17}cm^{-3}$). When light injected from *n*-side, the *n*-region surface recombination velocity affects detectivity when $n<10^{17}cm^{-3}$; the influence of thickness on detectivity is primarily when $n>10^{17}cm^{-3}$.

(Received January 20, 2015; accepted June 9, 2016)

Keywords: $In_{0.53}Ga_{0.47}As$ PV detector, Material parameters, Detectivity

1. Introduction

In recent year, due to the prominent features such as relatively low dark current density, quick response and high sensitivity and detectivity, $In_{1-x}Ga_xAs$ ternary alloys have become significant materials for the fabrication of infrared detectors. It has the same lattice constant as InP and room temperature energy bandgap of $0.73eV$ corresponding to a long wavelength cutoff 1.70 μm. The photovoltiac detectors made by Indium gallium arsenide ($In_{1-x}Ga_xAs$) have caused much attention in near infrared applications, such as optical fiber communication, spectroscope analysis and remote sensing, infrared imaging and many other fields [1-5].

Detectivity, denoted as D^* is an important parameter to measure detector performance. It is limited by quantum efficiency (η), dark current and zero bias resistance (R_0A) which are determined by material parameters of $In_{1-x}Ga_xAs$ ternary alloys. In this paper, we theoretically analysised the dependence of D^*, η and R_0A on the direction of incident light and material parameters which is carried out for a $In_{1-x}Ga_xAs$ photodetector lattice-matched to *InP*[6-10].

2. Theory analysis

The structure of photodetector is the homogenous *p-n* type of $In_{1-x}Ga_xAs$ deposited on *InP* substrate. Show in Fig. 1. The incident light is injected from the *n*-region or *p*-region. A two-dimensional model of detector is taken.

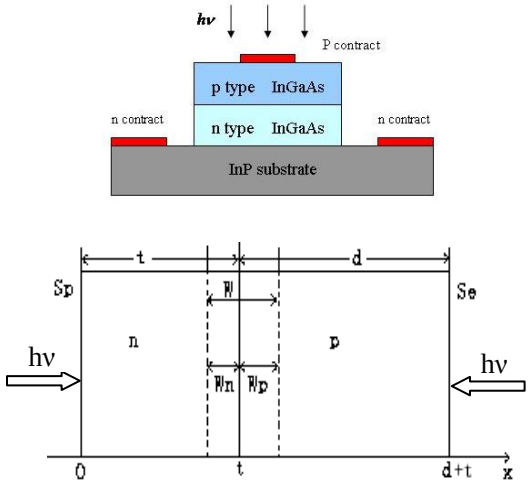

Fig. 1. Schematic 2D structure of $In_{1-x}Ga_xAs$ p-n junction

S_p and S_e is surface recombination velocity (*m/s*) for holes in *n* region and for electrons in *p* region; *t* and *d* are *n*-region width and *p*-region width; *n* and *p* are carrier concentration in *n*-region and *p*-region; *W* is width of depletion region; W_n is width of depletion region on *n* side; W_p is width of depletion region on *p* side. Usually, characterize the performance of Infrared photovoltaic detector by detectivity *D**, which depends on the zero-bias resistance-junction-area product (R_0A) and quantum efficiency, the equation of *D** is given by:

$$D^* = \frac{\lambda\eta q}{hc}\sqrt{\frac{R_0A}{4kT}} \tag{1}$$

where η and *k* are quantum efficiency the Boltzmann constant, *T* is the work temperature, λ is the wavelength of the incidence light, *q* is the charge of an electron and *c* is the velocity of light. In order to get the equation of η and R_0A, we must derive the equation of photocurrent. There are five basic equations [11]. They are two current density equations, two continuity equations for electron and hole in *p*-region and *n*-region respectively, and Poisson's equation:

current density for electrons: $J_e = qD_e\frac{dn}{dx} - q\mu_e n\frac{d\varphi}{dx}$

current density for holes: $J_h = -qD_h\frac{dp}{dx} - q\mu_h p\frac{d\varphi}{dx}$

continuity equation for electrons: $\frac{1}{q}\frac{dJ_e}{dx} + (G-R) = 0$

continuity equation for holes: $\frac{1}{q}\frac{dJ_h}{dx} - (G-R) = 0$

Poisson's equation: $\frac{d^2\varphi}{dx^2} = -\frac{q}{\varepsilon_0\varepsilon_S}(N_d - N_a + p - n)$

The photocurrent densities in different regions are obtained when the incident light is injected from the *n*-region. They are given by [12],

$$J_{n,ph} = \frac{\alpha qL_h(1-r)\varphi}{(\alpha^2L_h^{\ 2}-1)}\left\{\frac{(r_h+\alpha L_h) - e^{-\alpha(t-W_n)}[r_h\,\mathrm{ch}(\frac{t-w_n}{L_h}) + \mathrm{sh}(\frac{t-w_n}{L_h})]}{r_h\,\mathrm{sh}(\frac{t-w_n}{L_h}) + \mathrm{ch}(\frac{t-w_n}{L_h})} - \alpha L_h e^{-\alpha(t-W_n)}\right\} \tag{2}$$

$$J_{p,ph} = \frac{\alpha qL_e(1-r)\varphi}{(\alpha^2L_e^{\ 2}-1)}e^{-\alpha(t+W_p)}\left\{\alpha L_e + \frac{(r_e-\alpha L_e)e^{-\alpha(d-W_p)} - [r_e\,\mathrm{ch}(\frac{d-w_p}{L_e}) + \mathrm{sh}(\frac{d-w_p}{L_e})]}{r_e\,\mathrm{sh}(\frac{d-w_p}{L_e}) + \mathrm{ch}(\frac{d-w_p}{L_e})}\right\} \tag{3}$$

$$J_{dr,ph} = q\varphi(1-r)[e^{-\alpha(t-W_n)} - e^{-\alpha(t+W_p)}] \tag{4}$$

where $J_{n,ph}$, $J_{p,ph}$, and $J_{dr,ph}$ are photocurrent densities of *n*-region, *p*-region and depletion region, respectively. α、Φ、*r* are the absorption coefficient, light flux and reflection coefficient, respectively. $D_i = KT\mu_i / q$, $L_i = (D_i\tau_i)^{1/2}$ and $\gamma_i = L_iS_i/\mathrm{D_i}$, the angle mark *i* namely represents *e* or *h*. *L*, *S*, μ , *D* and τ are the diffusion length(*cm*)、surface recombination velocity(ms^{-1}), effective mobility($cm^2V^{-1}s^{-1}$), diffusion coefficient(cm^2s^{-1}), and carrier lifetime(s) respectively for holes in the *n* region or for electrons in the *p* region. n_i is the intrinsic carrier concentration (cm^{-3}), *p* or *n* is the major carrier concentration(cm^{-3}).

Therefore, the total photocurrent J_{ph} is given by:

$$J_{ph} = J_{n,ph} + J_{p,ph} + J_{dr,ph} \tag{5}$$

At the steady-state, the relation of total photocurrent density J_{ph} and total quantum efficiency η shows as following [13]:

$$J_{ph} = \eta q\varphi \tag{6}$$

The quantum efficiency of *n*-region, *p*-region and depletion region is derived from above equations.

$$\eta_n = \frac{\alpha L_h(1-r)}{(\alpha^2L_h^{\ 2}-1)}\left\{\frac{(r_h+\alpha L_h) - e^{-\alpha(t-W_n)}[r_h\,\mathrm{ch}(\frac{t-w_n}{L_h}) + \mathrm{sh}(\frac{t-w_n}{L_h})]}{r_h\,\mathrm{sh}(\frac{t-w_n}{L_h}) + \mathrm{ch}(\frac{t-w_n}{L_h})} - \alpha L_h e^{-\alpha(t-W_n)}\right\} \tag{7}$$

$$\eta_p = \frac{\alpha L_e(1-r)}{(\alpha^2L_e^{\ 2}-1)}\mathrm{e}^{-\alpha(t+W_p)}\left\{\alpha L_e + \frac{(r_e-\alpha L_e)\mathrm{e}^{-\alpha(d-W_p)} - [r_e\,\mathrm{ch}(\frac{d-w_p}{L_e}) + \mathrm{sh}(\frac{d-w_p}{L_e})]}{r_e\,\mathrm{sh}(\frac{d-w_p}{L_e}) + \mathrm{ch}(\frac{d-w_p}{L_e})}\right\} \tag{8}$$

$$\eta_{dr} = (1-r)[e^{-\alpha(t-W_n)} - e^{-\alpha(t+W_p)}] \quad (9)$$

$$\eta = \eta_n + \eta_p + \eta_{dr} \quad (10)$$

If light is injected from *p* region, the quantum efficiency of *n*-region, *p*-region, and depletion region is the same as (7)-(10), but corresponding parameter mark should be exchanged, that is $n \rightarrow p$, $r_e \rightarrow r_h$, $L_e \rightarrow L_h$, $W_p \rightarrow W_n$, $t \rightarrow d$, $p \rightarrow n$, $r_h \rightarrow r_e$, $L_h \rightarrow L_e$, $W_n \rightarrow W_p$, $d \rightarrow t$.

$R_0 A$ can be expressed as

$$\frac{1}{R} = \frac{dI}{dV}\Big|_{V=0} = A_e \frac{dJ}{dV}\Big|_{V=0} \quad (11)$$

A_e is device sectional area. Therefore the $R_0 A$ products in the *n* and *p* regions are given respectively by

$$(R_0 A)_e = \frac{kT}{q^2}\frac{L_e p}{D_e n_i^{\ 2}} \frac{r_e sh(\frac{d-w_p}{L_e}) + ch(\frac{d-w_p}{L_e})}{r_e ch(\frac{d-w_p}{L_e}) + sh(\frac{d-w_p}{L_e})} \text{ (p-region) (12)}$$

$$(R_0 A)_h = \frac{kT}{q^2}\frac{L_h n}{D_h n_i^{\ 2}} \frac{r_h sh(\frac{t-w_n}{L_h}) + ch(\frac{t-w_n}{L_h})}{r_h ch(\frac{t-w_n}{L_h}) + sh(\frac{t-w_n}{L_h})} \text{ (n-region) (13)}$$

The diffusion current contributions from the *n* and *p* regions are added to give the total diffusion current, and the total $R_0 A$ product from both sides is [14]

$$\frac{1}{(R_0 A)_{total}} = \frac{1}{(R_0 A)_e} + \frac{1}{(R_0 A)_p} \quad (14)$$

Material parameters of $In_{1-x}Ga_xAs$ ternary-alloy are calculated in this paper are obtained by method of linear interpolation. Related the material parameters are listed in Table 1.

Table 1. Material parameters used in this paper [15]

Alloy	*Eg(T)(eV)*	*Δ*	m_e^*/m_0	m_h^*/m_0	m_s^*/m_0	ε_r
GaAs	$1.519 - 5.4010^{-4} T^2/(T+204)$	*0.34*	*0.067*	*0.45*	*0.15*	*13.18*
InAs	$0.420 - 2.5010^{-4} T^2/(T+75)$	*0.38*	*0.023*	*0.41*	*0.089*	*14.5*

3. Results and analysis

We analyzed the influence of carrier concentrations, thickness, the surface recombination velocities in the two quasi-neutral regions and direction of incident light on detectivity. The calculation is performed on an $In_{0.53}Ga_{0.47}As$ PV detector operated at 300 *K*. In the calculation, the electron and hole mobility are μ_e=5000$cm^2/V \cdot s$ and μ_p=400$cm^2/V \cdot s$, respectively; the wavelength of the incident light is λ=1.4μm.

The wavelength and direction of incident light have a significant influence on the detectivity. Fig. 2 shows that the detectivity depends on the light wavelength and the incidence direction. It indicates that detectivity of light injected from the *p*-side is larger than the one injected from *n*-side at the same parameters. This can be explained that diffusion of minority carrier has impact on detectivity. The electronic diffusion length of the *p*-region is longer than holes' diffusion length of *n*-region, due to the mobility of electrons is higher than that of the holes. Therefore, when light is injected from the *p*-side, a larger number of minority carriers which generated by light absorption could arrived at *p*-*n* junction. The number is larger than that produced by light injected from the *n*-side. The electrons could be fully absorption in the quasi-neutral region. When light is incident from the *n*-region, the light intensity attenuation in *n* region firstly, and absorption in p-region is relatively smaller. These carriers contribute to photocurrent, which determine the Detectivity.

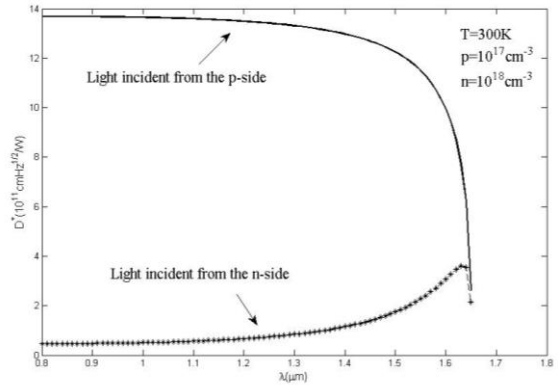

Fig. 2. Relationship between detectivity and direction of incident light with d=5μm, t=5μm, S_e=0, S_p=0, x=0.47.

Firstly, when light injected from *p*-side, the detectivity has been analyzed. Fig. 3 distinctly shows that detectivity versus the *p*-region carrier concentration (*p*) with the surface recombination velocity (S_e). The highest detectivity can be achieved 1.785×10^{12}cmHz$^{1/2}$/W when λ=1.4μm and *p* is at $10^{18}cm^{-3}$, which is consistent with experimental values reported by Antoni Rogalski [16]. The dependence of detectivity on carrier concentration with different surface recombination velocity has been researched. It obviously expresses that S_e has great effect on detectivity in the range of $p=10^{16}cm^{-3}$~$10^{19}cm^{-3}$, and detectivity has been decreased with increasing S_e. Furthermore, the detectivity of the device increases steadily with increase in doping concentration and reaches a peak value for different S_e and then finally decreases rather fast with a further increase in doping concentration. The largest value of detectivity has been received about $1.785\times10^{12}cmHz^{1/2}/W$ when the S_e for electrons is assumed to be zero. And the peak values are $1.704\times10^{12}cmHz^{1/2}/W$, $1.371\times10^{12}cmHz^{1/2}/W$ and $3.748\times10^{11}cmHz^{1/2}/W$ for S_e=100 (*m/s*), $S_e=10^4$ (*m/s*) and $S_e=10^8$ (*m/s*). Reducing surface recombination velocity is benefit to increasing detectivity. Therefore, to improve the performance of the detector, surface passivation processes are essential during device fabrication.

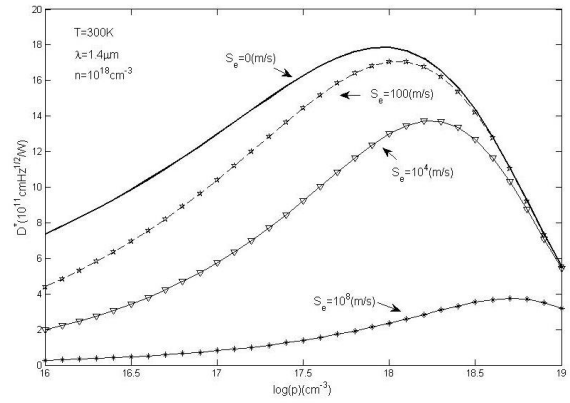

Fig. 3. The detectivity versus the p-side carrier concentration p with the S_e, d=5μm, t=5μm, S_p=0, x=0.47.

The effect of thickness (*d*) and surface recombination velocity (S_e) on detectivity is presented by Fig. 4. When $p=10^{18}cm^{-3}$ and d=5μm, relatively higher detectivity will be obtained ($D^*\approx1.8\times10^{12}cmHz^{1/2}/W$) in Fig. 4(a). Moreover, detectivity increases with thickness of *p*-region in the $log_{10}(p)$<17.8. When *p*-region is heavily doped about $log_{10}(p)$>18.8, detectivity for the narrow p-region thickness is larger than the one for wide p-region thickness. This conclusion has been confirmed in the literature of J. Kaniewski et al [17]. Furthermore, When $p=10^{18}cm^{-3}$, the detectivity appears a peak about $1.785\times10^{12}cmHz^{1/2}/W$ at d=5μm, and detectivity tends to decrease with increasing of *p*-side carrier concentration. For d=10μm and d=2μm, detectivity gradually increase and reach to peak about $1.753\times10^{12}cmHz^{1/2}/W$ and $1.371\times10^{12}cmHz^{1/2}/W$. It indicates that *p*-region carrier concentration around $10^{18}cm^{-3}$ will improve detectivity, which coincides with that in Fig. 3. Meanwhile, the *p*-region thickness needs to be adjusted to obtain high detectivity. Fig. 4 (b) provides the dependence of detectivity on *p*-region thickness (*d*) with different *p*-side surface recombination velocity (S_e). At the initial stage, detectivity is increasing with *d*, and arrives at largest value for different S_e. Subsequently, detectivity tends to be reduced. The highest detectivity is obtained for S_e=0 within d=6μm, which is about $2.362\times10^{12}cmHz^{1/2}/W$, and the peak value is got about $1.411\times10^{12}cmHz^{1/2}/W$ for $S_e=10^4m/s$ and about $0.239\times10^{12}cmHz^{1/2}/W$ for $S_e=10^8m/s$.

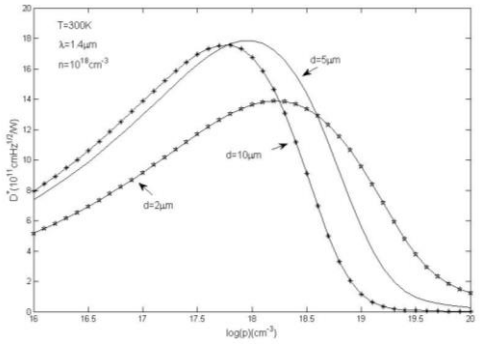

a

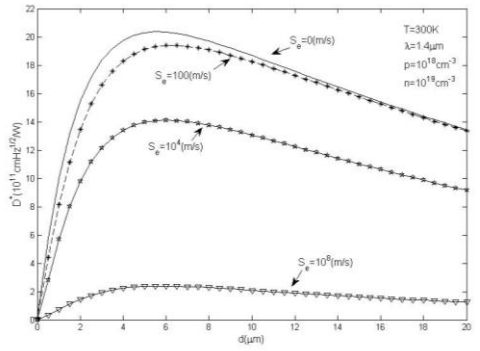

b

Fig. 4. (a) The detectivity versus the p-region carrier concentration with thickness of p-region. (b) The detectivity versus the thickness of p-region with different p-side surface recombination velocity at t = 5μm, S_p = 0, x=0.47

The relationship between the detectivity and *n*-region parameters has been provided in Fig. 5 at $p=10^{18}cm^{-3}$. The change of the detectivity with carrier concentration in *n*-region (*n*) as a function of *n*-side surface recombination velocity (S_p) has been shown in Fig. 5 (a). The detectivity versus carrier concentration in *n*-region with different *n*-region thickness (*t*) has been provided in Fig. 5 (b). The effect of *n*-region parameters on detectivity is smaller than the *p*-region parameters. Fig. 5 (a) explicitly expresses that detectivity drops with increasing S_p, but decreasing value gradually reduces with increasing *n*-region carrier concentrations. detectivity is nearly constant at large *n*-region carrier concentration. Furthermore, increasing *n*-region carrier concentrations makes detectivity augment, and detectivity can be obtained above $2\times10^{12}cmHz^{1/2}/W$ in $n\geq10^{19}cm^{-3}$. When $n\geq10^{18}cm^{-3}$, no matter what value of S_p has been taken, the value of detectivity keeps constant. Fig. 5 (b) depicts that the trend for detectivity at different thickness of *n*-region is similar. At the range of $10^{14}cm^{-3}<n<10^{19}cm^{-3}$, varied *t* has no influence on detectivity. However, detectivity appears slightly drop with decreasing *t* within $10^{14}cm^{-3}<n<10^{17}cm^{-3}$. Moreover, detectivity increases with increasing *n*, and detectivity achieves above $1.3\times10^{12}cmHz^{1/2}/W$ in $n>10^{18}cm^{-3}$. This phenomenon can be explained that the light is mainly absorbed in *p*-region, which leads the light intensity to be attenuated when light arrived at *n*-region. Therefore, the light absorption is reduced in *n*-region. It reflected that *n*-side surface recombination velocity and *n*-region thickness has fewer impacted on detectivity. In addition, the effect of S_p and *t* on detectivity is mainly in low carrier concentration of *n*-region. At range of high carrier concentration of *n*-region, the same detectivity has been achieved independent of S_p or *t*.

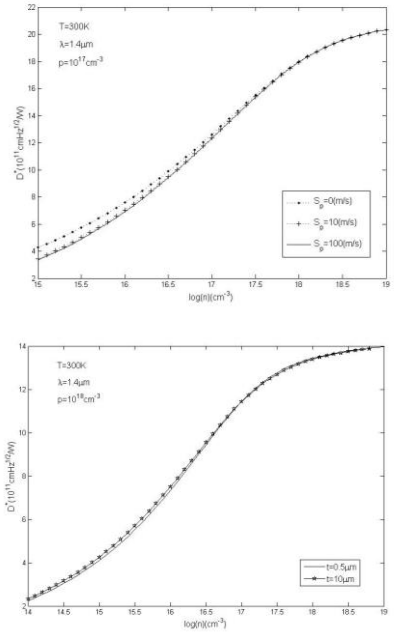

Fig. 5. (a) The detectivity versus carrier concentration in n-region with n-side surface recombination velocity at t=5μm. (b) The detectivity versus carrier concentration in n-region with the thickness of n-region at S_p=0. d=5μm, S_e=0, x=0.47

Furthermore, we have studied the dependence of detectivity on material parameters when incident light is injected from the *n*-region in Fig. 6. The relationship between detectivity and the *n*-region carrier concentration for different S_p is showed in Fig. 6 (a). It shows that the effect of surface recombination velocity on detectivity is primarily in $n<10^{17}cm^{-3}$ and the detectivity will be improved with the decrease of surface recombination velocity in *n*-region. When carrier concentration in *n*-region is $log_{10}(p)>16.5$, the detectivity has a stepwise decreases independent of S_p value. It can be explained that with increase of *n*-region carrier concentration, the diffusion length of *n*-region minority carrier is reduced, these minority carriers recombined before they arrived at *p*-*n* junction, thereby, detectivity is dropped. In addition, the increase of *n*-side surface recombination velocity leads to increase of the recombination of photo-generated minority carriers on surface. Therefore, the decrease of detectivity is due to the reducing number of minority carriers which arrived at *p*-*n* junction. Fig. 6 (b) shows the detectivity versus *n*-region carrier concentration with the thickness (*t*) as a parameter. It shows that the detectivity rapidly declines with increasing of *t* in $n>10^{16}cm^{-3}$. This can be attributed to that the diffusion length of *n*-region minority carrier becomes shorter with the *n*-region thickness increasing, therefore, the recombination of photo-generated carriers is increase, and consequently detectivity is reduced.

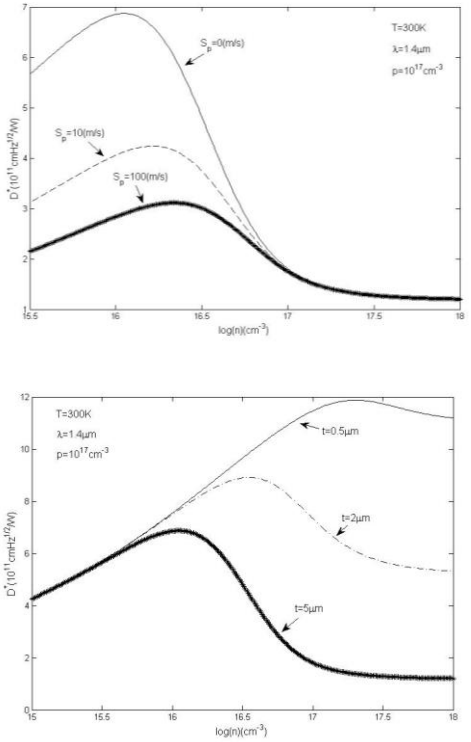

Fig. 6. (a) The relationship between detectivity and n-region carrier concentration for different S_p at t=5μm. (b) The dependence of detectivity on n-region carrier concentration with the thickness t as a parameter at S_p=0. d=5μm, S_e=0, x=0.47

4. Conclusion

In this paper, we analyzed the effect of carrier concentrations, thickness, surface recombination velocities in the two quasi-neutral regions and the direction of incident light on detectivity. It indicates that detectivity of light injected from the *p*-side is larger than the one injected from *n*-side at the same parameters. This can be explained that diffusion of minority carrier has impact on detectivity. When light is injected from *p*-side, *p*-region surface recombination velocity, *p*-region carrier concentration and *p*-region thickness have significant influence on detectivity. It concluded that high detectivity (D^*>1.8 × $10^{12} cmHz^{1/2}/W$) can be achieved, if *p*-region thickness is about $5\mu m$ for carrier concentration ($p=10^{17} cm^{-3}$). Furthermore, when *n*-region carrier concentration is about $n=10^{19} cm^{-3}$, quantum efficiency reaches to a peak value about $2.362\times10^{12} cmHz^{1/2}/W$ when the region thickness is about $d=6\mu$m. The material parameters of *n*-region have less effect on detectivity. The influence of S_p and t on detectivity is mainly at low carrier concentration of *n*-region ($n<10^{17} cm^{-3}$). When light is injected from *n*-side, the *n*-region surface recombination velocity affects detectivity mainly at $n<10^{17} cm^{-3}$; the influence of thickness on detectivity is mostly at $n>10^{17} cm^{-3}$. These results will provide benefit for designing and fabrication of the *InGaAs* PV detectors.

Acknowledgements

This work was supported by the key science and technology achievement transformation project of Jilin Province No. 20130303017GX. The key science and technology research project of Jilin Province No. 20140204028GX.

References

[1] L. C. Comandar, B. Frohlich, J. F. Dynes, A. W. Sharpe, M. Lucamarini Z. L. Yuan, R. V. Penty, A. J. Shields, Journal of Applied Physics. **117**, 083109 (2015).
[2] Fu Zheng, Feilong Wang, Chao Wang, Zhibin Sun, Guangjie Zhai, Nuclear Instruments and Methods in Physics Research Section A. **799**, 25 (2015).
[3] Yingtian Xu, Ying Li, Beihong Long, Yan Ma, Guotong Du, Jingzhi Yin, J. Optoelectron. Adv. M., **16**, 276 (2014).
[4] Yingtian Xu, Ying Li, Beihong Long, Yan Ma, Guotong Du, Jingzhi Yin, Optoelectron. Adv. Mat. **6**, 1009 (2012).
[5] Michael MacDougal, Jon Geske, Chad Wang, David Follman. Optical Engineering, **50**(6), 061011 (2011).
[6] Xiaofeng Duan, Yongqing Huang, Xiaomin Ren, Yufeng Shang, Xinye Fan, Fuquan Hu, IEEE Photonics Technology Letters, **24**(10), 863 (2012).
[7] Henry Yuan, Jongwoo Kim, Gary Apgar etal. Proc. of SPIE. **6950**, 695000 (2008).
[8] A. Tosi, F. Acerbi, A. Dalla Mora, M. A. Itzler, X. Jiang. IEEE Photonics Journal, **3**(1), 31 (2011).
[9] Lars Zimmermann, Joachim John, Stefan Degroote, Gustaaf Borghs, Chris Van Hoof, Appl. Phys. Lett. **82**, 2838 (2003).
[10] S. Ozer, O. O. Cellek, C. Besikci. Infrared Physics & Technology. **47**, 115 (2005).
[11] Y. Tian, Z. Tianming, Z. Baolin, J. Hong, J. Yixin. Solid-state Electronics, **43**, 625 (1999).
[12] P. Chakrabarti, P. K. Saxena, R. K. Lal, International Journal of Infrared and Millimeter Waves. **27**, 1119 (2006).
[13] R. K. Willardson, A. C. Beer, Semiconductors and Semimetals, Academic Press, United States, **18**, 201 (1981).
[14] V. Gopal, S. K. Singh, R. M. Mehra, Infrared Physics & Technology, **43**, 317 (2002).
[15] Yuchun Chang, Bao Shi, Longhai Li, Jingzhi Yin, Fubin Gao, Guotong Du, Yixin Jin, Solid State Communications, **151**, 1953 (2011).
[16] Antoni Rogalski, Infrared Physics & Technology, **43**, 187 (2002).
[17] J. Kaniewski, J. Piotrowski, Opto-Electronics Review, **12**(1), 139 (2004).

*Corresponding author: xuyingtian-007@163.com